Exact 3D elasticity solution for free vibrations of an eccentric hollow sphere

Seyyed M. Hasheminejad *, Yaser Mirzaei

Acoustics Research Laboratory, Department of Mechanical Engineering, Iran University of Science and Technology, Narmak, Tehran 16846-13114, Iran

ARTICLE INFO

ABSTRACT

An exact three-dimensional elastodynamic analysis for describing the natural oscillations of a freely suspended, isotropic, and homogeneous elastic sphere with an eccentrically located inner spherical cavity is developed. The translational addition theorem for spherical vector wave functions is employed to impose the zero traction boundary conditions, leading to frequency equations in the form of exact determinantal equations involving spherical Bessel functions and Wigner 3j symbols. Extensive numerical calculations have been carried out for the first five clusters of eigenfrequencies associated with both the axisymmetric and non-axisymmetric spheroidal as well as toroidal oscillation modes for selected inner-outer radii ratios in a wide range of cavity eccentricities. Also, the corresponding three-dimensional deformed mode shapes are illustrated in vivid graphical forms for selected eccentricities. The numerical results describe the imperative influence of cavity eccentricity, mode type, and radii ratio on the vibrational characteristics of the hollow sphere. The existence of "multiple degeneracies" and the trigger of "frequency splitting" are demonstrated and discussed. The accuracy of solution is checked through appropriate convergence studies, and the validity of results is established with the aid of a commercial finite element package as well as by comparison with the data in the existing literature.

1. Introduction

The dynamic behavior of shells has been a subject of study for more than a century, since they are extensively used as one of the basic components in civil, mechanical, aircraft, and naval structures. Many of these studies are based on classical or thin-shell theories, which utilize the well-known simplifying Kirchhoff–Love postulates of straight inextensional normal, making these theories inadequate for the analysis of thick shells. In recent years, the refinement of thin-shell theories has resulted in a number of the so-called higher order shell theories based on various approximations of shear deformation and rotary inertia associated with the transverse direction of the shell surface [1–3]. For dynamic analysis of complex structures, thin or higher order shell theories are most appropriate, but they lose their accuracy for thick structures, making the use of three-dimensional theory of elasticity inevitable. The high computational power requirements being the only limiting factor, the three-dimensional theory of elasticity may advantageously be used to accurately extract the full vibration spectrum of natural frequencies and mode shapes for simple geometries such as the solid or hollow elastic spheres and cylinders without any missing modes. Such analysis, not only provides reliable solutions for benchmarking purposes, but also can bring out the physical characteristics of the problem.

* Tel.: +98912 7371354; fax: +9821 77240488.
  E-mail address: hashemi@iust.ac.ir (S.M. Hasheminejad).

Natural vibration of freely suspended solid and thick hollow elastic spheres has long been one of the fundamental problems in elastodynamics, originally associated with interest in the oscillations of the earth [4]. Numerous researchers have carried out three-dimensional analysis based on the linear equations of elasticity in order to find accurate natural frequencies for the vibrations of solid or hollow thick spheres. Restricting our attention to the purely isotropic problems, the most important works relevant to the present study will briefly be reviewed here. The first known complete mathematical treatment for the vibrations of an ideal isotropic elastic sphere was given by Lamb [5] in Cartesian coordinates and by Chree [6] in the more convenient spherical coordinates. In particular, Lamb [5] presented two basic types of free vibrations: torsional (toroidal or equivoluminal) vibrations or vibrations of the first class associated with the rotatory motions of the sphere where there is no change in volume of the sphere and no radial displacement; and spheroidal (pulsating or coupled bending–stretching) vibrations or vibrations of the second class which are related to the distortion of the elastic sphere due to vibrations in the radial direction. Most of the subsequent studies were based on the work of Lamb and driven by the interest in understanding the generation of earthquakes and their effect on earth. For instance, Sato and Usami [7,8] performed a detailed spectral analysis and provided (tabulated) a comprehensive set of results for the frequencies of free vibration and their corresponding displacement field distributions within vibrating homogeneous elastic spheres. Subsequently Shah et al. [9] studied the free vibrational behavior of hollow spheres by using an exact three-dimensional analysis to obtain a characteristic equation solvable in terms of spherical Bessel functions of the first and second kind and gave numerical results for a wide range of thickness to radius ratios in graphical form. Extensive work on the vibration of spheres including complicating effects, such as anisotropic material properties, liquid core, multi-layers and self-gravitation effects, has been carried out by numerous researchers. An excellent reference on the subject is the very readable book by Lapwood and Usami [10]. Hosseini-Hashemi and Anderson [11] examined issues of normalization of the torsional vibration characteristics of solid elastic spheres and presented three-dimensional diagrams for the surface displacement of the toroidal modes. Heyliger and Jilani [12] used the Ritz method to verify the results of Sato and Usami [7,8] for isotropic spheres and gave some results for inhomogeneous spheres as well as an excellent list of references. Kumbasar [13] used three-dimensional elastodynamic equations to study free vibrations of complete thick spherical shells. Chang and Demkowicz [14] determined natural frequencies of a vibrating hollow, elastic sphere using both the 3D elasticity and Kirchhoff shell theory. McGee and Spry [15] used a complete set of algebraic trigonometric polynomials to approximate the radial, meridional, and circumferential displacements (via Ritz method) to address the spheroidal and toroidal elastic vibrations of thick-walled, spherical bodies of revolution based on the three-dimensional theory of elasticity in curvilinear coordinates. Chau [16] used two scalar wave potentials to derive the exact frequency equation and numerical results for only the toroidal mode of vibrations for a spherically isotropic elastic sphere. Buchanan and Rich [17] formulated a finite element model to study the effects of the boundary conditions on free vibration of thick isotropic spherical shells. Saviot and Murray [18] presented a qualitative distinction between different spheroidal modes of vibration of a free continuum elastic sphere. Duffey et al. [19] compared natural frequencies and mode shapes obtained from axisymmetric and non-axisymmetric theories of vibration of complete free spherical shells with those from finite element computer simulations with and without geometrical imperfections.

Analytical solutions of interior or exterior boundary value problems in different fields such as potential theory, acoustics, elastodynamics, and electromagnetism are stringently dependent on the shape of boundaries. In particular, when multiple (eccentric) interfaces are present in a wave field, there is an interaction between them due to cross scattering. The theoretical basis for the solution of the wave interaction problems involving eccentric spherical boundaries was set by Friedman and Russek [20], Stein [21] and Cruzan [22], who provided the translational addition theorems for spherical wave functions. After that, several researchers have studied the eccentric sphere problem. Among them, Golovchan [23] considered axisymmetric forced oscillations of (dynamic stress concentrations within) an elastic sphere with a non-concentric inner cavity under the action of a uniform external pressure. Kanellopoulos and Fikioris [24] obtained the natural frequencies for the scalar interior boundary value problem in the acoustic region between two eccentric spherical surfaces, for both Neumann and Dirichlet boundary conditions. Roumeliotis et al. [25] and Roumeliotis and Kanellopoulos [26] employed a special shape perturbation method to derive analytical expressions for the acoustic resonance frequency shifts in a hard- (soft-) walled spherical cavity, caused by introduction of an eccentric small inner sphere. Roumeliotis et al. [27] used spherical vector wave functions and related addition theorems to derive analytical expressions for the resonant frequencies in an electromagnetic spherical cavity with an eccentric inner electrically small and perfectly conducting sphere for both the magnetic and electric modes. Roumeliotis et al. [28] used the classical method of separation of variables combined with translational addition theorems for spherical vector wave functions to treat the scattering of a plane electromagnetic wave from a metallic or dielectric sphere of electrically small radius, embedded into a dielectric one. Cottis and Moyssidis [29] investigated the effect of eccentricity on the complex resonances of a conducting sphere eccentrically coated by a dielectric one. Charalambopoulos et al. [30] used the elasticity theory in conjunction with the bispherical coordinates system to study the effect of the thickness nonuniformities of the human dry skull (modeled by an isotropic elastic material occupying the region bounded by two non-concentric spheres) on its frequency spectrum. Their analysis is however independent of the azimuthal coordinate (i.e., perfectly axisymmetric), and is only valid for small deviations of the system from the concentric case. Ioannidou and Chrissoulidis [31] obtained an exact solution to the problem of electromagnetic-wave scattering from a sphere with an arbitrary number of non-overlapping spherical inclusions by use of the indirect mode-matching technique. Videen [32] derived the scattered fields from a spherical body eccentrically located within an otherwise homogeneous host sphere due to an arbitrarily positioned seismic source,
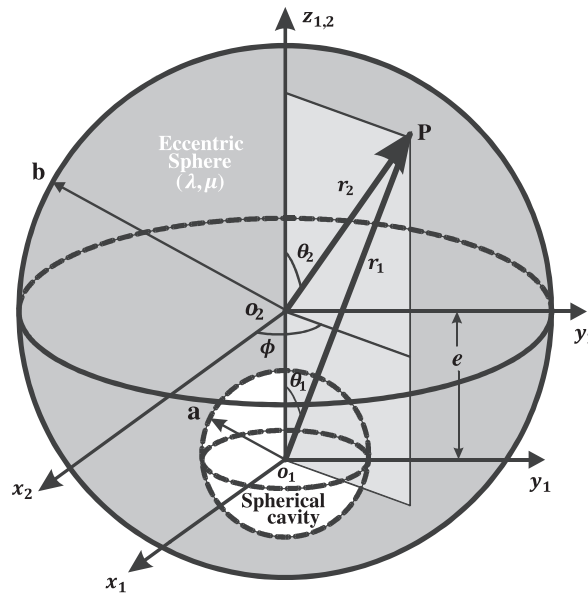
Fig. 1. The problem geometry.

composed of any linear combination of S and P waves. Hasheminejad and Azarpeyvand [33] offered an exact study on radiation of an acoustic field due to modal vibrations of a spherical source, eccentrically positioned within a thermoviscous fluid sphere, into an external boundless viscous thermally conducting fluid medium. Moneda and Chrissoulidis [34] developed an exact, analytical solution to the problem of electric point source radiation in the presence of a sphere with an eccentric spherical inclusion (cavity) by combined use of the dyadic Green's function formalism and the indirect mode-matching technique. Han et al. [35] utilized the rotational addition theorems for spherical vector wave functions in conjunction with the approach of the localized approximation to investigate the far-field electromagnetic-wave scattering of an eccentric sphere arbitrarily located in a shaped optical beam. Just recently, Yan et al. [36] employed addition theorem for spherical vector wave functions to study the interaction between a Gaussian beam and an arbitrarily positioned sphere with an eccentric inclusion in the framework of generalized Lorenz–Mie theory (GLMT).

The above review clearly indicates that, while there exists a notable body of acoustic- or electromagnetic-oriented literature tackling the eccentric sphere problem, a rigorous three-dimensional elastodynamic (free vibration) analysis of this problem (see Fig. 1) appears to be nonexistent. Accordingly, the main purpose of the current work is to employ the translational addition theorem for spherical vector wave functions [22] along with the appropriate orthogonal series expansions and the pertinent boundary conditions to develop an exact three-dimensional elasticity solution for the anticipated problem. The proposed full three-dimensional model can support a rich variety of oscillation modes which is of fundamental interest as a canonical problem in structural dynamics. The presented exact solution can form an invaluable guide for design engineers in assessing the effects of introducing cavity eccentricity (shell wall non-uniformity) on the frequency response of such structures in various physical and technological applications [30,37–39]. It can particularly complement experimental procedures for detection or identification of internal nonuniformities in precision spherical components, as an effective means to characterize and control the quality of the specimen [40–42]. The accurately extracted full vibration spectrum of natural frequencies and mode shapes can serve as the benchmark for the evaluation of other solutions obtained by merely numerical or approximate approaches [43]. It can also serve as the prerequisite to examining the transient response characteristics of eccentric elastic spheres [44].

2. Formulation

2.1. Basic field equations

The elastic material under consideration is assumed to be linear, macroscopically homogeneous, and isotropic. In the absence of body forces, the displacement field is governed by the classical Navier's equation [45]

$$\rho \frac{\partial^2 \mathbf{u}}{\partial t^2} = \mu \nabla^2 \mathbf{u} + (\lambda + \mu) \nabla(\nabla \cdot \mathbf{u}), \tag{1}$$

subject to the appropriate boundary conditions. Here, (λ, μ) are Lame constants, ρ is the solid material density, and $\mathbf{u}$ is the vector displacement that can advantageously be decomposed as the sum of an irrotational part $\mathbf{u}'$, corresponding to a

compressional wave, and a solenoidal part $\mathbf{u}''$, corresponding to a shear wave [9]:

$$\mathbf{u} = \mathbf{u}' + \mathbf{u}'', \tag{2}$$

where $\nabla \cdot \mathbf{u}'' = 0$, $\nabla \times \mathbf{u}' = 0$. The above decomposition enables one to separate the dynamic equation of motion (1) into the decoupled vector Helmholtz equations:

$$\nabla^2 \mathbf{u}' + \alpha^2 \mathbf{u}' = 0,$$
$$\nabla^2 \mathbf{u}'' + \beta^2 \mathbf{u}'' = 0, \tag{3}$$

where ∇^2 is the Laplacian, $\alpha^2 = \omega^2/c_p^2$, $\beta^2 = \omega^2/c_s^2$, and $c_p^2 = (\lambda + 2\mu)/\rho$ and $c_s^2 = \mu/\rho$ are the propagation velocities of dilatational and distortional waves in the elastic medium, respectively. The solutions of the vector Helmholtz equations (3) may be written as [9]

$$\mathbf{u}' = \mathbf{L} = \nabla\varphi$$
$$\mathbf{u}'' = \mathbf{M} + \mathbf{N} = \nabla \times (\mathbf{e}_r r\psi) + \nabla \times \nabla \times (\mathbf{e}_r r\chi) \tag{4}$$

where the displacement potentials (φ, ψ, χ) satisfy the scalar Helmholtz equations:

$$(\nabla^2 + \alpha^2)\varphi = 0,$$
$$(\nabla^2 + \beta^2)(\psi, \chi) = 0. \tag{5}$$

2.2. Field expansions and boundary conditions

The problem geometry is depicted in Fig. 1. Two spherical coordinate systems (r_1, θ_1, ϕ_1) and (r_2, θ_2, ϕ_2) are introduced as shown in the figure to describe the elastic field within the eccentric sphere. The spherical coordinates have same meridional angle $\phi_1 = \phi_2 = \phi$. Their origin-to-origin separation is e, and point P is an arbitrary field point within the eccentric sphere, outside the spherical cavity. Keeping the decomposition (2) in mind, while taking advantage of the solutions of the scalar Helmholtz equations (5) in (4), the field expansions for the displacement components within the eccentric sphere may be written with respect to the (r_1, θ_1, ϕ) coordinate system as [46]

$$\mathbf{u}(r_1, \theta_1, \phi, \omega) = \sum_{n=0}^{\infty} \sum_{m=-n}^{n} [a_{nm} \mathbf{L}_{mn}^{[1]}(r_1, \theta_1, \phi, \omega) + b_{nm} \mathbf{L}_{mn}^{[2]}(r_1, \theta_1, \phi, \omega) + c_{nm} \mathbf{M}_{mn}^{[1]}(r_1, \theta_1, \phi, \omega)$$
$$+ d_{nm} \mathbf{M}_{mn}^{[2]}(r_1, \theta_1, \phi, \omega) + e_{nm} \mathbf{N}_{mn}^{[1]}(r_1, \theta_1, \phi, \omega) + f_{nm} \mathbf{N}_{mn}^{[2]}(r_1, \theta_1, \phi, \omega)] \tag{6}$$

where a_{nm} through f_{nm} are unknown modal coefficients, and the appropriate expressions for $\mathbf{L}_{mn}^{[i]}(r_j, \theta_j, \phi, \omega)$, $\mathbf{M}_{mn}^{[i]}(r_j, \theta_j, \phi, \omega)$ and $\mathbf{N}_{mn}^{[i]}(r_j, \theta_j, \phi, \omega)(j, i = 1, 2)$ are given in Appendix A [46]. Consequently, the relevant displacement components are written in the form

$$u_r(r_1, \theta_1, \phi, \omega) = \sum_{n=0}^{\infty} \sum_{m=-n}^{n} [a_{nm} V_{1n}^{[1]} + b_{nm} V_{1n}^{[2]} + e_{nm} V_{3n}^{[1]} + f_{nm} V_{3n}^{[2]}] P_n^m(\cos\theta_1) e^{im\phi},$$

$$u_\theta(r_1, \theta_1, \phi, \omega) = \sum_{n=1}^{\infty} \sum_{m=-n}^{n} \left[(c_{nm} V_{5n}^{[1]} + d_{nm} V_{5n}^{[2]}) \frac{i\,m}{\sin\theta_1} P_n^m(\cos\theta_1) + (a_{nm} V_{4n}^{[1]} + b_{nm} V_{4n}^{[2]} + e_{nm} V_{6n}^{[1]} + f_{nm} V_{6n}^{[2]}) \frac{\partial P_n^m(\cos\theta_1)}{\partial\theta_1} \right] e^{i\,m\phi},$$

$$u_\phi(r_1, \theta_1, \phi, \omega) = \sum_{n=1}^{\infty} \sum_{m=-n}^{n} \left[-(c_{nm} V_{5n}^{[1]} + d_{nm} V_{5n}^{[2]}) \frac{\partial P_n^m(\cos\theta_1)}{\partial\theta_1} + (a_{nm} V_{4n}^{[1]} + b_{nm} V_{4n}^{[2]} + e_{nm} V_{6n}^{[1]} + f_{nm} V_{6n}^{[2]}) \frac{i\,m}{\sin\theta_1} P_n^m(\cos\theta_1) \right] e^{i\,m\phi}, \tag{7}$$

where $i = \sqrt{-1}$, P_n^m are the associated Legendre functions [47], and $V_{in}^{[k]}(r_j, \omega)$ $(i = 1, 2, \ldots, 6; \quad j, k = 1, 2)$ are given in Appendix B. Also, the stress tensor may be written in terms of the displacement vector as [45]

$$\boldsymbol{\sigma} = \lambda(\boldsymbol{\nabla} \cdot \mathbf{u})\mathbf{I} + \mu(\nabla\mathbf{u} + \mathbf{u}\nabla) \tag{8}$$

where $\mathbf{I}$ is the unitary dyadic. Therefore, the pertinent stress components can be written in the form

$$\sigma_{rr}(r_1, \theta_1, \phi, \omega) = \sum_{n=0}^{\infty} \sum_{m=-n}^{n} [a_{nm} S_{1n}^{[1]} + b_{nm} S_{1n}^{[2]} + c_{nm} S_{2n}^{[1]} + d_{nm} S_{2n}^{[2]} + e_{nm} S_{3n}^{[1]} + f_{nm} S_{3n}^{[2]}] P_n^m(\cos\theta_1) e^{i\,m\phi},$$

$$\sigma_{r\theta}(r_1, \theta_1, \phi, \omega) = \sum_{n=1}^{\infty} \sum_{m=-n}^{n} \left[(c_{nm} S_{5n}^{[1]} + d_{nm} S_{5n}^{[2]}) \frac{i\,m}{\sin\theta_1} P_n^m(\cos\theta_1) + (a_{nm} S_{4n}^{[1]} + b_{nm} S_{4n}^{[2]} + e_{nm} S_{6n}^{[1]} + f_{nm} S_{6n}^{[2]}) \frac{\partial P_n^m(\cos\theta_1)}{\partial\theta_1} \right] e^{i\,m\phi},$$

$$\sigma_{r\phi}(r_1, \theta_1, \phi, \omega) = \sum_{n=1}^{\infty} \sum_{m=-n}^{n} \left[-(c_{nm} S_{5n}^{[1]} + d_{nm} S_{5n}^{[2]}) \frac{\partial P_n^m(\cos\theta_1)}{\partial\theta_1} + (a_{nm} S_{4n}^{[1]} + b_{nm} S_{4n}^{[2]} + e_{nm} S_{6n}^{[1]} + f_{nm} S_{6n}^{[2]}) \frac{i\,m}{\sin\theta_1} P_n^m(\cos\theta_1) \right] e^{i\,m\phi}, \tag{9}$$

where the expressions for $S_{in}^{[k]}(r_j, \omega)$ $(i = 1, 2, \ldots, 6; \quad j, k = 1, 2)$ are given in Appendix B.

The natural frequencies and the unknown Fourier coefficients may be determined by imposing the proper boundary conditions. Accordingly, assuming traction-free inner and outer surfaces, one can write (see Fig. 1)

$$\sigma_{rr}(r_1 = a, \theta_1, \phi, \omega) = \sigma_{r\theta}(r_1 = a, \theta_1, \phi, \omega) = \sigma_{r\phi}(r_1 = a, \theta_1, \phi, \omega) = 0, \tag{10a}$$

$$\sigma_{rr}(r_2 = b, \theta_2, \phi, \omega) = \sigma_{r\theta}(r_2 = b, \theta_2, \phi, \omega) = \sigma_{r\phi}(r_2 = b, \theta_2, \phi, \omega) = 0. \tag{10b}$$

Using (9) along with the classical orthogonality properties of spherical harmonics and their derivatives with respect to the θ_j-coordinate [48] in (10a), after some relatively tedious manipulations, one obtains two distinct sets of equations for the meridional mode numbers $m=0$ and $m \neq 0$ at $r_1=a$:

m=0:

$$a_{n0}S_{1n}^{[1]}(a,\omega) + b_{n0}S_{1n}^{[2]}(a,\omega) + e_{n0}S_{3n}^{[1]}(a,\omega) + f_{n0}S_{3n}^{[2]}(a,\omega) = 0,$$
$$a_{n0}S_{4n}^{[1]}(a,\omega) + b_{n0}S_{4n}^{[2]}(a,\omega) + e_{n0}S_{6n}^{[1]}(a,\omega) + f_{n0}S_{6n}^{[2]}(a,\omega) = 0, \quad c_{n0}S_{5n}^{[1]}(a,\omega) + d_{n0}S_{5n}^{[2]}(a,\omega) = 0, \tag{11}$$

where $n = 0,1,2,\ldots$.

m≠0:

$$a_{nm}S_{1n}^{[1]}(a,\omega) + b_{nm}S_{1n}^{[2]}(a,\omega) + e_{nm}S_{3n}^{[1]}(a,\omega) + f_{nm}S_{3n}^{[2]}(a,\omega) = 0, \tag{12a}$$

$$i\, m\Lambda_1(a,n,m,\omega) + \Lambda_2(a,n+1,m,\omega)\kappa(n+1,m) + \Lambda_2(a,n-1,m,\omega)\gamma(n-1,m)(1-\delta_{nm}) = 0, \tag{12b}$$

$$i\, m\Lambda_2(a,n,m,\omega) - \Lambda_1(a,n+1,m,\omega)\kappa(n+1,m) - \Lambda_1(a,n-1,m,\omega)\gamma(n-1,m)(1-\delta_{nm}) = 0, \tag{12c}$$

where $n=m$, $m+1$, $m+2$, $\ldots$. Also, the expressions for $(\Lambda_1, \Lambda_2, \kappa, \gamma)$ along with the procedure for enforcement of the last two boundary conditions in (10a) for the case $m \neq 0$ (i.e., obtaining Eqs. 12b and 12c) is outlined in the Appendix C. On the other hand, exact satisfaction of the outer boundary condition (10b) is a far more intricate matter, which will be achieved next by application of the translational addition theorem for the spherical vector wave functions.

2.3. Translational vector addition theorem

Many problems involve wave fields of one characteristic shape (coordinate system) that interact with a boundary of some other shape (coordinate system). So it is difficult to satisfy the boundary conditions on that surface. There exists, however, a particular class of mathematical relationships called translational addition theorems that circumvent this difficulty in many cases by allowing one to study various wave fields with respect to a common origin. To fulfill orthogonality in the current problem (see Fig. 1), we shall employ Cruzan's [22] formulation of translational addition theorem for spherical vector wave functions to expand solutions of the vector Helmholtz equations with respect to the first coordinate system (r_1, θ_1, ϕ) (i.e., Eq. (6)) in terms of the second coordinate system (r_2, θ_2, ϕ). Noting that the two spherical coordinate systems share the same z-axis (see Fig. 1), after some manipulations, Cruzan's formulation can favorably be simplified for the given problem in the form (see also [49]):

$$\mathbf{L}_{mn}^{[j]}(r_1,\theta_1,\phi,\omega) = \sum_{\nu=m}^{\infty} Z_{m\nu}^{mn}(e,\omega)\mathbf{L}_{mn}^{[j]}(r_2,\theta_2,\phi,\omega)$$

$$\mathbf{M}_{mn}^{[j]}(r_1,\theta_1,\phi,\omega) = \sum_{\nu=m}^{\infty} Q_{m\nu}^{mn}(e,\omega)\mathbf{M}_{mn}^{[j]}(r_2,\theta_2,\phi,\omega) + R_{m\nu}^{mn}(e,\omega)\mathbf{N}_{mn}^{[j]}(r_2,\theta_2,\phi,\omega)$$

$$\mathbf{N}_{mn}^{[j]}(r_1,\theta_1,\phi,\omega) = \sum_{\nu=m}^{\infty} Q_{m\nu}^{mn}(e,\omega)\mathbf{N}_{mn}^{[j]}(r_2,\theta_2,\phi,\omega) + R_{m\nu}^{mn}(e,\omega)\mathbf{M}_{mn}^{[j]}(r_2,\theta_2,\phi,\omega) \tag{13}$$

where $r_2 > e$, $j=1,2$, and the pertinent expressions for the translation coefficients $(Z_{m\nu}^{mn}, Q_{m\nu}^{mn}, R_{m\nu}^{mn})$ are given in Appendix D. Accordingly, the expansions (13) can be utilized in (6) in order to express the field displacement with respect to second coordinate system as

$$\mathbf{u}(r_2,\theta_2,\phi,\omega) = \sum_{n=0}^{\infty}\sum_{m=-n}^{n} [A_{nm}\mathbf{L}_{mn}^{[1]}(r_2,\theta_2,\phi,\omega) + B_{nm}\mathbf{L}_{mn}^{[2]}(r_2,\theta_2,\phi,\omega) + C_{nm}\mathbf{M}_{mn}^{[1]}(r_2,\theta_2,\phi,\omega)$$
$$+ D_{nm}\mathbf{M}_{mn}^{[2]}(r_2,\theta_2,\phi,\omega) + E_{nm}\mathbf{N}_{mn}^{[1]}(r_2,\theta_2,\phi,\omega) + F_{nm}\mathbf{N}_{mn}^{[2]}(r_2,\theta_2,\phi,\omega)] \tag{14}$$

where expressions for the coefficients $A_{nm}(e,\omega)$ through $F_{nm}(e,\omega)$ are given in Appendix E. Also, direct substitution of field expansions (14) into the stress–displacement relation (8), leads to the expressions for stress components with respect to the second coordinate system:

$$\sigma_{rr}(r_2,\theta_2,\phi,\omega) = \sum_{n=0}^{\infty}\sum_{m=-n}^{n} \left[A_{nm}S_{1n}^{[1]} + B_{nm}S_{1n}^{[2]} + C_{nm}S_{2n}^{[1]} + D_{nm}S_{2n}^{[2]} + E_{nm}S_{3n}^{[1]} + F_{nm}S_{3n}^{[2]} \right] P_n^m(\cos\theta_2)e^{i\,m\phi},$$

$$\sigma_{r\theta}(r_2,\theta_2,\phi,\omega) = \sum_{n=1}^{\infty}\sum_{m=-n}^{n} \left[(C_{nm}S_{5n}^{[1]} + D_{nm}S_{5n}^{[2]})\frac{i\,m}{\sin\theta_2}P_n^m(\cos\theta_2) + (A_{nm}S_{4n}^{[1]} + B_{nm}S_{4n}^{[2]} + E_{nm}S_{6n}^{[1]} + F_{nm}S_{6n}^{[2]})\frac{\partial P_n^m(\cos\theta_2)}{\partial\theta_2} \right] e^{i\,m\phi},$$

$$\sigma_{r\phi}(r_2,\theta_2,\phi,\omega) = \sum_{n=1}^{\infty} \sum_{m=-n}^{n} \left[-(C_{nm}S_{8n}^{[1]} + D_{nm}S_{8n}^{[2]})\frac{\partial P_n^m(\cos\theta_2)}{\partial\theta_2} + (A_{nm}S_{7n}^{[1]} + B_{nm}S_{7n}^{[2]} + E_{nm}S_{9n}^{[1]} + F_{nm}S_{9n}^{[2]})\frac{\mathrm{i}\,m}{\sin\theta_2}P_n^m(\cos\theta_2) \right] e^{\mathrm{i}\,m\phi},$$

(15)

At this point, by going through the same procedure as for enforcement of the inner boundary condition (10a), one can impose the outer surface condition (10b) to obtain the following complementary equations for the meridional mode number $m=0$ and $m\neq0$ at $r_2=b$:

m=0:

$$A_{n0}S_{1n}^{[1]}(b,\omega) + B_{n0}S_{1n}^{[2]}(b,\omega) + E_{n0}S_{3n}^{[1]}(b,\omega) + F_{n0}S_{3n}^{[2]}(b,\omega) = 0,$$
$$A_{n0}S_{4n}^{[1]}(b,\omega) + B_{n0}S_{4n}^{[2]}(b,\omega) + E_{n0}S_{6n}^{[1]}(b,\omega) + F_{n0}S_{6n}^{[2]}(b,\omega) = 0,$$
$$C_{n0}S_{5n}^{[1]}(b,\omega) + D_{n0}S_{5n}^{[2]}(b,\omega) = 0,$$

(16)

For $n=0,1,2,\dots;$.

m≠0:

$$A_{nm}S_{1n}^{[1]}(b,\omega) + B_{nm}S_{1n}^{[2]}(b,\omega) + E_{nm}S_{3n}^{[1]}(b,\omega) + F_{nm}S_{3n}^{[2]}(b,\omega) = 0,$$
$$\mathrm{i}m\Gamma_1(b,e,n,m,\omega) + \Gamma_2(b,e,n+1,m,\omega)\kappa(n+1,m) + \Gamma_2(b,e,n-1,m,\omega)\gamma(n-1,m)(1-\delta_{nm}) = 0,$$
$$\mathrm{i}m\Gamma_2(b,e,n,m,\omega) - \Gamma_1(b,e,n+1,m,\omega)\kappa(n+1,m) - \Gamma_1(b,e,n-1,m,\omega)\gamma(n-1,m)(1-\delta_{nm}) = 0,$$

(17)

where $n=m, m+1, m+2, \dots;$ and

$$\Gamma_1(b,e,n,m,\omega) = C_{nm}S_{5n}^{[1]}(b,\omega) + D_{nm}S_{5n}^{[2]}(b,\omega),$$
$$\Gamma_2(b,e,n,m,\omega) = A_{nm}S_{4n}^{[1]}(b,\omega) + B_{nm}S_{4n}^{[2]}(b,\omega) + E_{nm}S_{6n}^{[1]}(b,\omega) + F_{nm}S_{6n}^{[2]}(b,\omega)$$

Now, simultaneous solutions of infinite-order systems (11) and (16) for $m=0$, and (12) and (17) for $m\neq0$, are, respectively, required for complete dynamic characterization of the problem. For the $m=0$ mode, taking $n=0,1,2,\dots,N$, the linear system of Eqs. (11) and (16) may advantageously be truncated into the matrix form:

$$\mathbf{T}_0\mathbf{c}_0 = \mathbf{0},$$

(18)

where $\mathbf{T}_0$ is a $(6N+1)\times(6N+1)$ square matrix that contains extremely complicated frequency-dependent parameters which multiply the modal vector $\mathbf{c}_0$, and

$$\mathbf{c}_0 = [a_{00},b_{00},c_{00},d_{00},e_{00},f_{00}; a_{10},b_{10},c_{10},d_{10},e_{10},f_{10}; \quad \dots; a_{N0},b_{N0},c_{N0},d_{N0},e_{N0},f_{N0}]^T$$

Similarly, for the $m\neq0$ mode, taking $n=m, m+1, m+2, \dots, m+N$, the linear system of Eqs. (12) and (17) may expediently be truncated into the matrix form:

$$\mathbf{T}_m\mathbf{c}_m = 0,$$

(19)

where $\mathbf{T}_m$ is a $6N\times6N$ square matrix that contains extremely complicated frequency-dependent parameters which multiply the modal vector $\mathbf{c}_m$, and

$$\mathbf{c}_m = [a_{mm},b_{mm},c_{mm},d_{mm},e_{mm},f_{mm}; a_{(m+1),m},b_{(m+1)m},c_{(m+1)m},d_{(m+1)m},e_{(m+1)m},f_{(m+1)m};$$
$$\dots; a_{(m+N)m},b_{(m+N)m},c_{(m+N)m},d_{(m+N)m},e_{(m+N)m},f_{(m+N)m}]^T$$

Lastly, for nontrivial solutions of systems (18) and (19), the associated determinants, $|\mathbf{T}_0|$ and $|\mathbf{T}_m|$ must, respectively, be set equal to zero, leading to the final frequency equations. The resonant frequencies must be obtained numerically by searching for the real roots of these equations. Here, it is noteworthy that in the concentric sphere case ($e=0$) with $m=0$, the oscillation equations (18) may readily be decoupled into two independent systems of equations representing the purely spheroidal and purely toroidal modes, and that these equations get coupled only through the effects of introducing eccentricity. For $m\neq0$ (non-axisymmetric) modes, on the other hand, the specially complex internal structure of the truncated oscillation equations (19) does not allow decoupling into two independent systems of equations corresponding to the spheroidal and toroidal modes, even in the concentric case. This completes the necessary background required for exact analysis of the problem. Next, we consider some numerical examples.

3. Numerical results

In order to illustrate the nature and general behavior of solution, we consider a number of numerical examples in this section. A Mathematica code [50] was constructed for numerical treatment of the systems (18) and (19), i.e., to calculate the resonance frequencies and to determine the unknown Fourier coefficients (mode shapes) as a function of the dimensionless (cavity) eccentricity parameter $\bar{e} = (b-a)/b$. In particular, a simple and very efficient root finding technique based on the bisection approach is employed to determine the roots of the characteristic equations ($|\mathbf{T}_0|=0, |\mathbf{T}_m|=0$), by performing tedious frequency sweeping with extremely small frequency steps for detection of the value of the frequency parameters that cause the determinant to change sign. This procedure was repeated for all eccentricities using very small eccentricity steps ($\Delta\bar{e}\approx 1\%$). This way, any remaining missing frequencies were identified and immediately included. Also, after finding the roots of the characteristic equations by the above mentioned procedure,

each root is substituted back into the coefficient matrices ($\mathbf{T}_0, \mathbf{T}_m$) and the corresponding eigenvector is obtained by using the powerful Mathematica built-in function "Nullspace." The computations were performed on a network of personal computers with a maximum truncation constant of $v_{max} = n_{max} = N = 30$ to assure convergence in the high frequency range, and also in case of high core eccentricity. The convergence of numerical solutions were systematically checked in a simple trial and error manner, by increasing the truncation constant (i.e., including higher number of modes) while looking for steadiness or stability in the numerical value of the solutions.
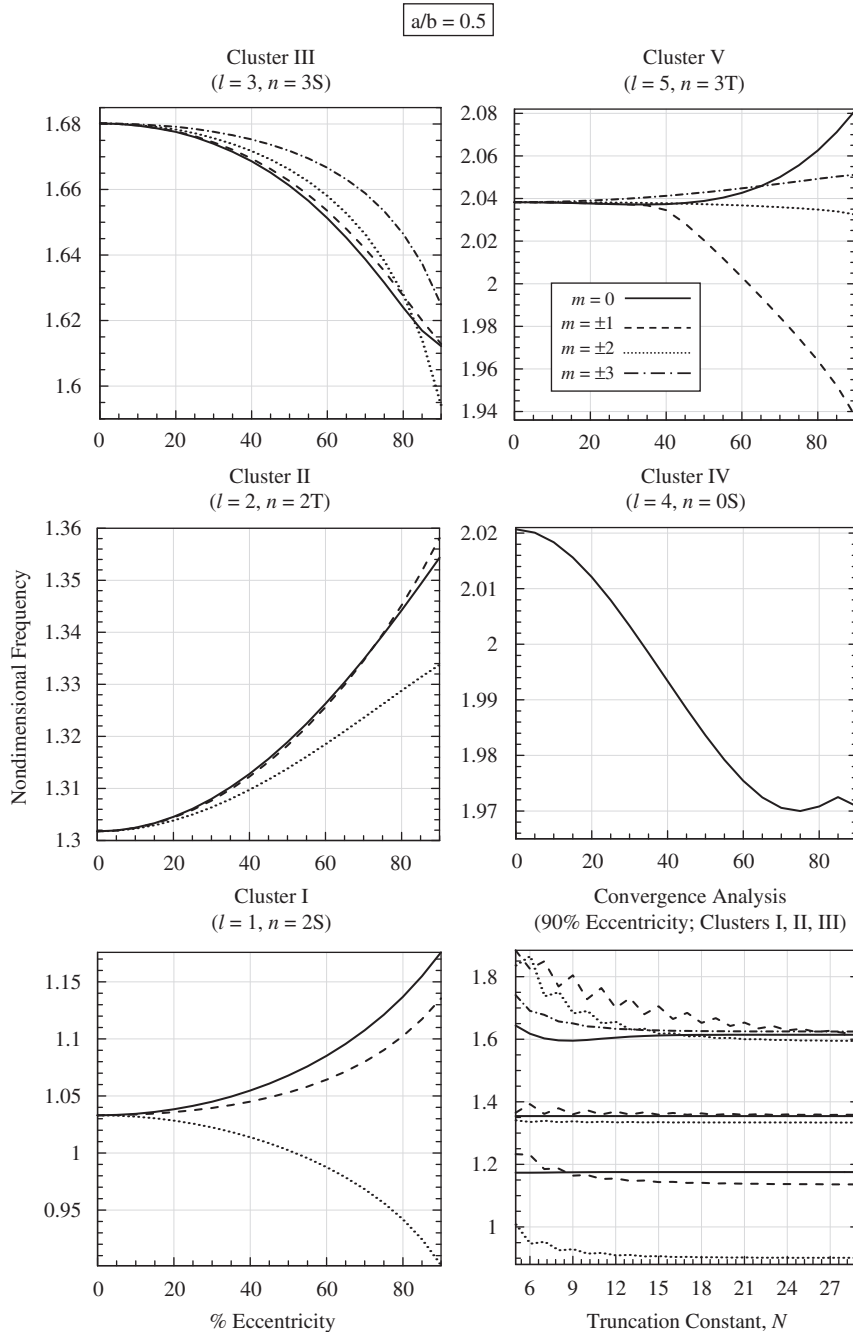
Figs. 2 through 4 display the variation of the first five clusters of dimensionless natural frequencies ($\Omega = \omega b/c_p$) with the eccentricity parameter $0 \leq \bar{e} = (b-a)/b \leq 0.9$ for the selected inner–outer radius ratios of $a/b = 0.2, 0.5, 0.9$. The associated root or cluster number (l), and the azimuthal and meridional mode numbers (n, m) are also specified. Also, the frequency
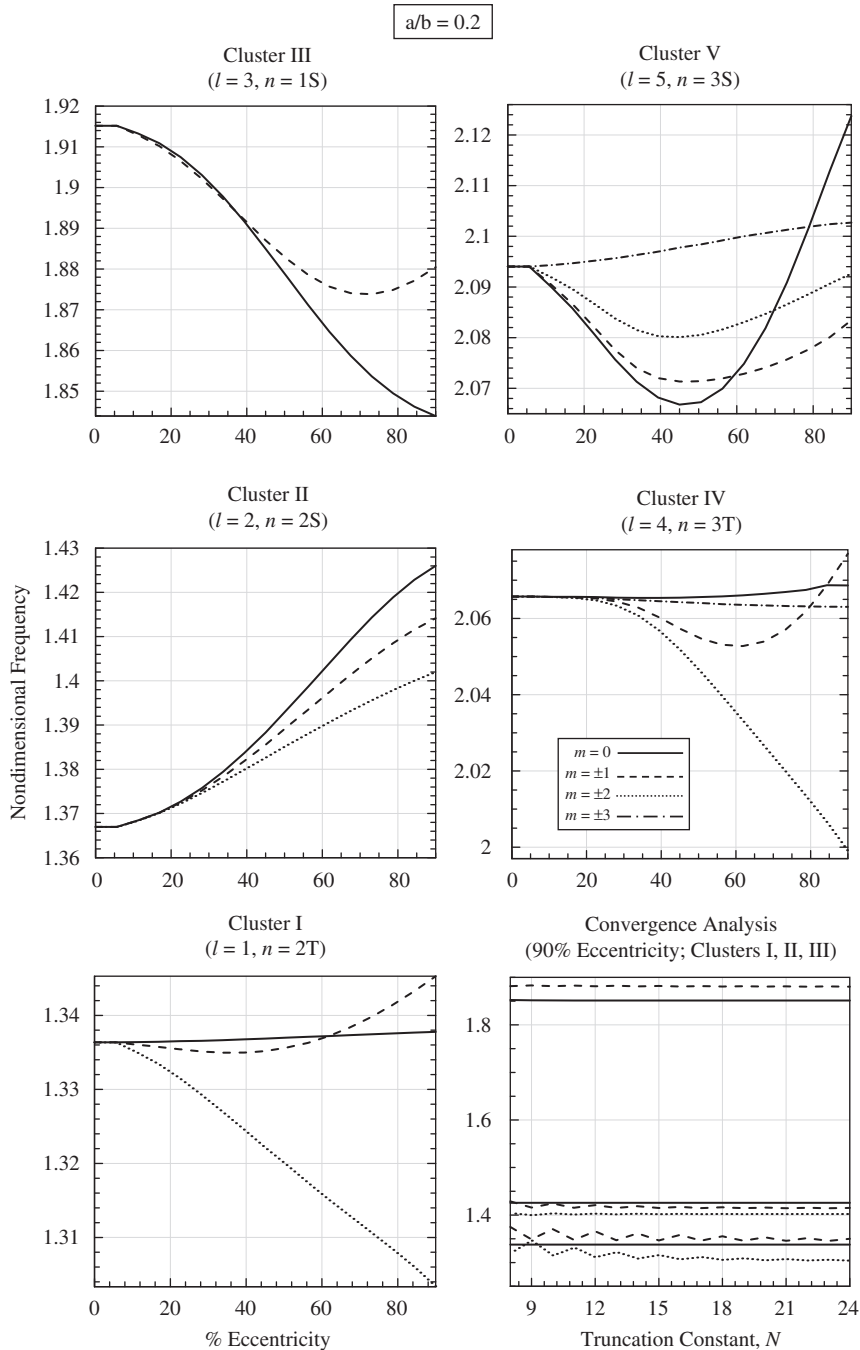
Fig. 2. The variation of the first five clusters of dimensionless natural frequencies ($\Omega = \omega b/c_p$) with the eccentricity parameter along with the relevant convergence analysis for the selected inner–outer radius ratios of $a/b = 0.2$.

spectrum clusters associated with the purely spheroidal and purely toroidal oscillation modes in the concentric sphere situation, are specified with the letters "S" and "T", respectively. Also shown in lower right corner of each figure is the corresponding variation of the first few clusters of natural frequencies with the truncation constant, N, for the most critical situation, i.e., for the sphere with the highest eccentricity ($\bar{e} = 90\%$). Here, it is clear that the adopted truncation constant of $N_{max}=30$ well assures the adequate convergence of all calculated natural frequencies. The modal spectrums of eccentric spheres exhibit very unique characteristics. In the absence of eccentricity ($e=0$), the spheroidal and toroidal modes are completely decoupled [15], and for each value of n (azimuthal number) and l (root or "cluster" number), because of the perfect azimuthal and meridional symmetries, a total of $2n+1$ perfectly repeated fully degenerate (multiplet) frequencies is observed (i.e., there is $2n+1$-fold degeneracy; see Ref. [19]). For example, considering the fifth frequency cluster associated
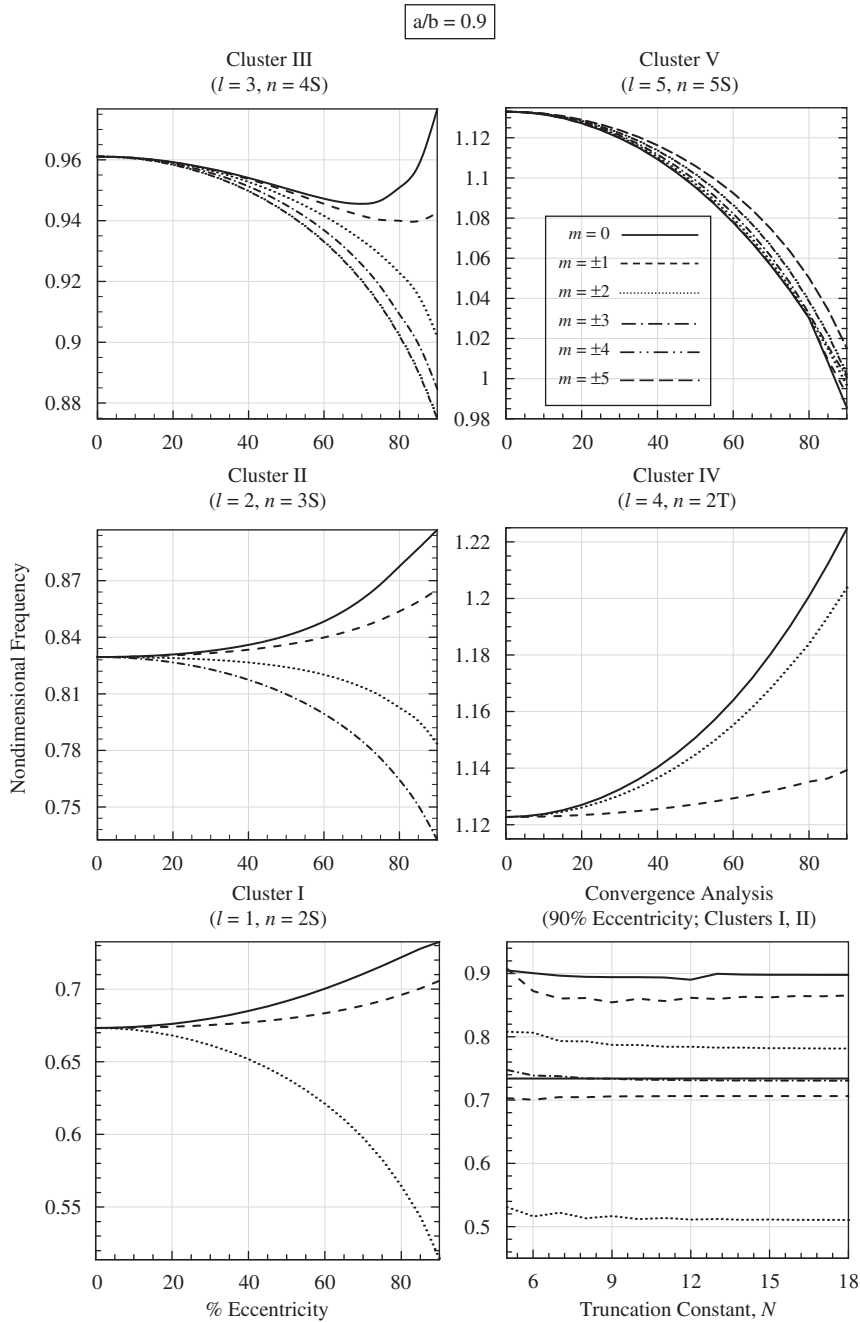

Fig. 3. The variation of the first five clusters of dimensionless natural frequencies ($\Omega=\omega b/c_p$) with the eccentricity parameter along with the relevant convergence analysis for the selected inner–outer radius ratios of a/b=0.5.

with the purely spheroidal mode in the concentric case (l=5; n=3S), there is a total of $2n$+1=7 fully degenerate frequencies, with m=0, $\pm$1, $\pm$2, $\pm$3.

The eccentricity parameter inflicts characteristically different effects on natural frequencies depending on the radii ratio and mode number. In particular, as the cavity becomes eccentric (i.e., the azimuthal symmetry is lost; see Fig. 1), the problem is no longer fully degenerate, and n+1 of these $2n$+1 repeated vibration frequencies split into distinct eigenfrequencies. However, n frequencies within the $2n$+1 frequencies remain two-fold degenerate (i.e., we get the so-named paired eigenmodes: m= $\pm$1, $\pm$2, $\pm$3,...). For example, reconsidering the fifth frequency cluster (l=5;n=3S) in Fig. 2, the previously $2n$+1=7 fully degenerate frequencies in the concentric case, now form a cluster with n+1=4 distinct branches, n=3 of which are two-fold degenerate (i.e., m= $\pm$1, $\pm$2, $\pm$3). Also, it is clear from the various subplots in each figure that besides splitting of eigenfrequencies, the numerous crossovers of different branches occur. In particular, one can

Fig. 4. The variation of the first five clusters of dimensionless natural frequencies (Ω=$\omega b/c_p$) with the eccentricity parameter along with the relevant convergence analysis for the selected inner–outer radius ratios of a/b=0.9.

clearly observe internal crossovers between clusters I, III, IV, V in Fig. 2; internal crossovers between clusters II, III, V and external crossovers between clusters IV,V in Fig. 3; internal crossovers in cluster V and external crossovers between clusters II, III, and IV, V in Fig. 4. Also, it appears that the number of (internal) frequency crossover points increases as the radii ratio is decreased. At these crossovers, corresponding to specific eccentricities, the previously split eigenfrequencies become degenerate. This implies that beyond the crossover eccentricity, the stiffness of structure in one vibration mode will interchange place with another. Furthermore, it is interesting to note that, regardless of radii ratio, the frequency spectrum curve associated with the $n=0$ (breathing) mode remains single-valued in the entire range of eccentricity (e.g., see Fig. 3; cluster IV). In other words, there is a single non-degenerate frequency associated with the breathing mode regardless of cavity eccentricity. Moreover, comparison of Figs. 2 through 4 indicates the general increase of the natural frequency with the increase of shell wall thickness. Lastly, it appears that the largest overall shift in natural frequencies due to the increase in eccentricity occurs at highest radii ratio ($a/b=0.9$).

Fig. 5 displays the three dimensional deformed mode shapes associated with the first five clusters of dimensionless frequencies for selected eccentricity parameters ($\bar{e} = 0, 30, 60, 90\%$). Also, the associated natural frequencies are listed in Table 1. Comments very similar to above remarks can readily be made. The main distinctions are as follows. Here it is clear that for a fixed azimuthal mode number n and increasing order (meridional mode number) $-n \leq m \leq n$, there are a total of $2n+1$ modes, $n+1$ of which are perfectly distinct. Among this $n+1$ perfectly distinct modes, n modes which occur in pairs are identical in shape differing only in orientation (note that the rotated mode shapes are not shown in the figures for brevity). This means that, when $m=0$ there is only one associated mode shape and when $m \neq 0$ there are two independent
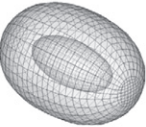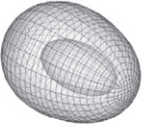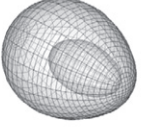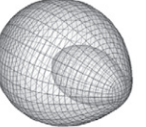

Fig. 5. Selected three dimensional deformed mode shapes associated with the first five clusters of dimensionless frequencies for various eccentricity parameters.
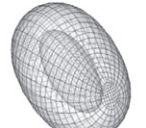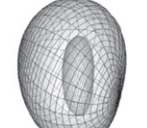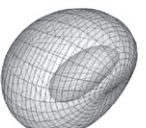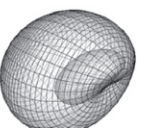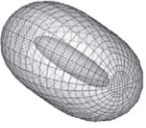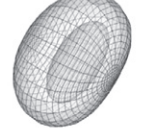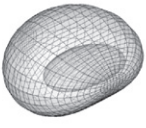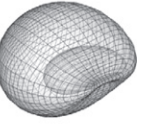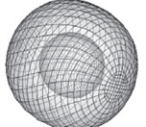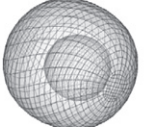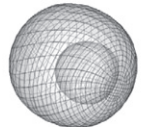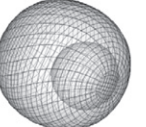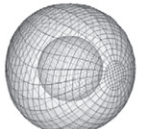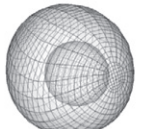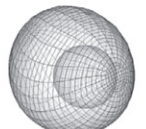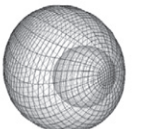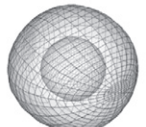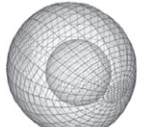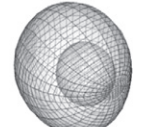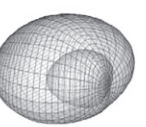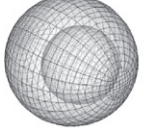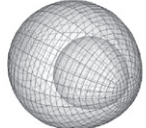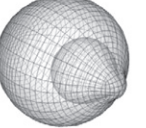
n	m	0% Eccentricity	30% Eccentricity	60% Eccentricity	90%Eccentricity
3S	0				
	±1				
	±2				
	±3				
3T	0				
	±1				
	±2				
	±3				

Fig. 5. (*Continued*)

mode shapes occurring in pairs with the same frequency. Here, it should be reminded that, as discussed earlier, in the concentric case all of the $2n+1$ modes are linked with the fully degenerate frequencies (see Table 1), while in the eccentric sphere situations, the n paired modes possess two-fold degenerate frequencies. Lastly, it is interesting to note that as the cavity eccentricity increases, the geometric "imperfection" becomes significant, the mode shapes illustrated in the first column of Fig. 5 ($\bar{e} = 0$) become gradually more corrupted. This change in deformed mode shapes, which is of maximum effect in case of the sphere with the highest eccentricity ($\bar{e} = 90\%$), may directly be linked to the previously discussed "splitting" of originally degenerate modes.

Finally, in order to check overall validity of the work, we first used our general Mathematica code to compute the first five clusters of natural frequencies, $f=\omega/2\pi$ (Hz), associated with three dimensional deformed mode shapes pre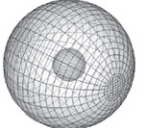sented in Fig. 5, for a very thick steel sphere (a=0.1 m, b=0.2 m, E=2 $\times$ 10^{11} N/m^2, ρ=7800 kg/m^3, v=0.3). Table 1 clearly indicates that our exact calculations exhibit excellent agreements with the numerical computations made by using the commercial finite element code ABAQUS/Standard Version 6.6 [51]. It is noteworthy that in the latter validations, a total of about 7000 twenty-noded brick elements "C3D20R" of ABAQUS were used to model the eccentric sphere problem. As a further check, we set e=0 in our general code in order to compare our calculated results with approximate numerical results presented in Ref. [15] for a concentric hollow sphere, in which excellent agreements were found (comparisons are not displayed for briefness). Lastly, we compared the results computed through our Mathematica code with the approximate results presented in Ref. [30] for free (axisymmetric) vibrations of an elastic sphere of non-uniform wall thickness. Owing to various approximations made in the latter reference, good agreements were found only for the case of extremely small deviations from the concentric case (comparisons are not shown for brevity).

Table 1
Comparison of the analytically calculated natural frequencies, $f=\omega/2\pi$ (Hz), with the numerical computations made by using the FEM code ABAQUS for selected eccentricity parameters ($\bar{e}=$ 0,30,60,90%) of a hollow steel sphere.

n	m	%Eccentricity							
		0%		30%		60%		90%	
		Analytical	FEM	Analytical	FEM	Analytical	FEM	Analytical	FEM
2	0	4829.74	4829.81	4885.41	4885.53	5072.94	5073.46	5496.07	5497.54
	± 1	4829.74	4829.94	4859.77	4859.97	4975.46	4975.74	5310.71	5308.99
		4829.74	4829.94	4859.77	4859.97	4975.46	4975.74	5310.71	5309.00
	± 2	4829.74	4830.11	4779.47	4779.87	4616.25	4616.69	4212.87	4213.30
		4829.74	4830.13	4779.47	4779.88	4616.25	4616.70	4212.87	4213.30
2	0	6086.0	6086.05	6115.14	6115.12	6200.65	6200.64	6331.81	6331.81
	± 1	6086.0	6086.15	6113.61	6113.70	6197.64	6197.73	6349.82	6349.47
		6086.0	6086.15	6113.61	6113.70	6197.64	6197.73	6349.82	6349.47
	± 2	6086.0	6086.35	6107.70	6107.98	6164.59	6164.87	6236.14	6235.97
		6086.0	6086.36	6107.70	6107.99	6164.59	6164.88	6236.14	6235.97
3	0	7854.93	7855.07	7825.70	7825.86	7720.83	7720.17	7538.43	7537.32
	± 1	7854.93	7855.27	7827.71	7828.16	7730.04	7730.54	7544.00	7540.29
		7854.93	7855.27	7827.71	7828.16	7730.04	7730.54	7544.00	7540.33
	± 2	7854.93	7855.88	7833.53	7834.60	7750.90	7752.28	7454.83	7451.09
		7854.93	7855.93	7833.53	7834.67	7750.90	7752.40	7454.83	7451.1
	± 3	7854.93	7857.05	7842.91	7845.12	7791.62	7793.86	7596.54	7596.63
		7854.93	7857.05	7842.91	7845.13	7791.62	7793.86	7596.54	7596.63
0	0	9447.18	9447.32	9366.27	9366.10	9235.51	9235.75	9223.82	9213.73
	0	9529.30	9529.43	9524.33	9524.46	9549.76	9549.88	9615.64	9623.64
3	± 1	9529.30	9529.42	9524.45	9524.57	9364.55	9364.71	9062.43	9058.01
		9529.30	9529.42	9524.45	9524.57	9364.55	9364.71	9062.43	9058.03
	± 2	9529.30	9529.88	9528.06	9528.64	9522.16	9522.74	9502.57	9501.95
		9529.30	9529.94	9528.06	9528.69	9522.16	9522.79	9502.57	9501.96
	± 3	9529.30	9530.75	9537.20	9538.63	9559.80	9552.93	9589.94	9589.91
		9529.30	9530.75	9537.20	9538.63	9559.80	9552.93	9589.94	9589.91

4. Conclusions

The translational addition theorem for spherical vector wave functions is employed to formulate the first known full 3D exact elasticity solution for the free vibration problem of an eccentric hollow elastic sphere. Accurate extensive 3D reference data are offered, which can serve as a benchmark to check the accuracy of various approximate theories. In particular, the first five clusters of resonant frequencies are calculated as a function of cavity eccentricity for selected geometric parameters. Also, selected three-dimensional deformed mode shapes are illustrated in vivid graphical forms. The most important observations are summarized as follows.

- In the absence of eccentricity, the spheroidal and toroidal modes are completely decoupled, and for each value of n (azimuthal number) and l (cluster number), due to the perfect azimuthal and meridional symmetries, there are $2n+1$-fold degenerate frequencies, regardless of the meridional mode number $-n \leq m \leq n$.
- The eccentricity parameter inflicts characteristically different effects on natural frequencies depending on the radii ratio and mode numbers. As the cavity becomes eccentric, the problem is no longer fully degenerate, and $n+1$ of the initial $2n+1$ degenerate frequencies split into distinct frequencies. However, n frequencies within the $n+1$ frequencies remain two-fold degenerate. In other words, there are n paired eigenfrequencies with $m= \pm 1, \pm 2, \pm 3, …, \pm n$ and one single frequency with $m=0$. In particular, for the breathing ($n=0$) mode, there is a single non-degenerate frequency regardless of cavity eccentricity.
- Besides splitting of eigenfrequencies, several (internal/external) crossovers of different branches are observed to occur. At these crossover eccentricities, the previously split eigenfrequencies become degenerate, and beyond the crossovers, the stiffness of structure in one vibration mode trades place with another.
- The largest overall shift in the natural frequencies due to the increase in cavity eccentricity occurs at the highest radii ratio, and there is a general rise of the eigenfrequencies with the increase of shell wall thickness.
- Regardless of cavity eccentricity, it is found that for each mode number n, there are a total of $2n+1$ free oscillation mode shapes with $-n \leq m \leq n$, $n+1$ of which are perfectly distinct within which n mode shapes occur in pairs (i.e., $m= \pm 1, \pm 2, \pm 3, …, \pm n$). In other words, when $m=0$ there is only one mode shape, while for $m \neq 0$ there are two mode shapes, occurring in pairs with the same degenerate frequency, identical in shape differing only in orientation.
- As the cavity eccentricity (geometric imperfection) increases, the deformed mode shapes are observed to become gradually more corrupt, which is directly linked to the "splitting" of the initially degenerate eigenfrequencies.

Appendix A

$$\mathbf{L}_{mn}^{[k]}(r_i,\theta_i,\phi,\omega) = \left[\frac{\partial}{\partial r_i}\left[\ell_n^{[j]}(\alpha r_i)\right]P_n^m(\cos\theta_i)\mathbf{e}_{r_i} + \frac{1}{r_i}\ell_n^{[j]}(\alpha r_i)\frac{\partial P_n^m(\cos\theta_i)}{\partial\theta_i}\mathbf{e}_{\theta_i} + \frac{\mathrm{i}\,m}{\sin\theta_i}\ell_n^{[j]}(\alpha r_i)P_n^m(\cos\theta_i)\mathbf{e}_\phi\right]e^{\mathrm{i}\,m\phi}$$

$$\mathbf{M}_{mn}^{[j]}(r_i,\theta_i,\phi,\omega) = \left[\frac{\mathrm{i}\,m}{\sin\theta_i}\ell_n^{[j]}(\beta r_i)P_n^m(\cos\theta_i)\mathbf{e}_{\theta_i} - \ell_n^{[j]}(\beta r_i)\frac{\partial P_n^m(\cos\theta_i)}{\partial\theta_i}\mathbf{e}_\phi\right]e^{\mathrm{i}\,m\phi}$$

$$\mathbf{N}_{mn}^{[j]}(r_i,\theta_i,\phi,\omega) = \left[\frac{n(n+1)}{r_i}\ell_n^{[j]}(\beta r_i)P_n^m(\cos\theta_i)\mathbf{e}_r + \frac{1}{r_i}\frac{\partial}{\partial r_i}\left[r_i\ell_n^{[j]}(\beta r_i)\right]\frac{\partial P_n^m(\cos\theta_i)}{\partial\theta_i}\mathbf{e}_{\theta_i} + \frac{\mathrm{i}\,m}{r_i\sin\theta_i}\frac{\partial}{\partial r_i}\left[r_i\ell_n^{[j]}(\beta r_i)\right]P_n^m(\cos\theta_i)\mathbf{e}_\phi\right]e^{\mathrm{i}\,m\phi}$$

where $i,k=1,2$; and

$$\ell_n^{[k]} = \begin{cases} j_n & (k=1) \\ y_n & (k=2) \end{cases},$$

in which j_n and y_n are the spherical Bessel functions of the first and second kind [47], respectively.

Appendix B

$$V_{1n}^{[i]}(r_j,\omega) = \frac{\partial}{\partial r_j}\ell_n^{[i]}(\alpha r_j), \quad V_{2n}^{[i]}(r_j,\omega) = 0, \quad V_{3n}^{[i]}(r_j,\omega) = \frac{n(1+n)}{r_j}\ell_n^{[i]}(\beta r_j), \quad V_{4n}^{[i]}(r_j,\omega) = \frac{1}{r_j}\ell_n^{[i]}(\alpha r_j),$$

$$V_{5n}^{[i]}(r_j,\omega) = \ell_n^{[i]}(\beta r_j), \quad V_{6n}^{[i]}(r_j,\omega) = \frac{1}{r_j}\frac{\partial}{\partial r_j}\left[r_j\ell_n^{[i]}(\beta r_j)\right],$$

$$S_{1n}^{[i]}(r_j,\omega) = \left[2\mu\frac{n(n-1)}{r_j^2} - (\lambda+2\mu)\alpha^2\right]\ell_n^{[i]}(\alpha r_j) + 4\mu\frac{\alpha}{r_j}\ell_{n+1}^{[i]}(\alpha r_j),$$

$$S_{2n}^{[i]}(r_j,\omega) = 0,$$

$$S_{3n}^{[i]}(r_j,\omega) = 2\mu n(n+1)\left[\frac{(n-1)}{r_j^2}\ell_n^{[i]}(\beta r_j) - \frac{\beta}{r_j}\ell_{n+1}^{[i]}(\beta r_j)\right],$$

$$S_{4n}^{[i]}(r_j,\omega) = 2\mu\left[-\frac{(n-1)}{r_j^2}\ell_n^{[i]}(\alpha r_j) + \frac{\alpha}{r_j}\ell_{n+1}^{[i]}(\alpha r_j)\right],$$

$$S_{5n}^{[i]}(r_j,\omega) = \mu\left[\frac{(n-1)}{r_j}\ell_n^{[i]}(\beta r_j) - \beta\ell_{n+1}^{[i]}(\beta r_j)\right],$$

$$S_{6n}^{[i]}(r_j,\omega) = \mu\left[\left(\frac{2(1-n^2)}{r_j^2} + \beta^2\right)\ell_n^{[i]}(\beta r_j) - 2\frac{\beta}{r_j}\ell_{n+1}^{[i]}(\beta r_j)\right],$$

Appendix C

The derivative of associated Legendre functions may be written in the form [47]:

$$\frac{\partial}{\partial\theta}\left[P_n^m(\cos\theta)\right] = \csc\theta\left[\frac{(n+m)(-n-1)}{2n+1}P_{n-1}^m(\cos\theta) + \frac{n(n-m+1)}{2n+1}P_{n+1}^m(\cos\theta)\right].$$

By using the above expansion in second of (9), the boundary condition $\sigma_{r\theta}(r_1=a,\theta_1,\phi,\omega)=0$ in (10a) can be rewritten as

$$\sigma_{r\theta}(a,\theta_1,\phi,\omega) = \sum_{n=1}^\infty \sum_{m=-n}^n \left\{\Lambda_1(a,n,m,\omega)\frac{\mathrm{i}\,m}{\sin\theta_1}P_n^m(\cos\theta_1)\right.$$
$$\left. + \Lambda_2(a,n,m,\omega)\csc\theta_1[\kappa(n,m)P_{n-1}^m(\cos\theta_1) + \gamma(n,m)P_{n+1}^m(\cos\theta_1)]\right\}e^{\mathrm{i}\,m\phi} = 0, \tag{C1}$$

where

$$\kappa(n,m) = \frac{(n+m)(-n-1)}{2n+1}, \quad \gamma(n,m) = \frac{n(n-m+1)}{2n+1},$$
$$\Lambda_1(r_1,n,m,\omega) = c_{nm}S_{5n}^{[1]}(r_1,\omega) + d_{nm}S_{5n}^{[2]}(r_1,\omega),$$
$$\Lambda_2(r_1,n,m,\omega) = a_{nm}S_{4n}^{[1]}(r_1,\omega) + b_{nm}S_{4n}^{[2]}(r_1,\omega) + e_{nm}S_{6n}^{[1]}(r_1,\omega) + f_{nm}S_{6n}^{[2]}(r_1,\omega),$$

Next, by employing the classical orthogonality of exponential functions (see Eq. 12.141 in Ref. [48]), Eq. (C1) can be expanded in the following form:

$$\sum_{n=m}^\infty \Lambda_1(a,n,m,\omega)\frac{\mathrm{i}\,m}{\sin\theta_1}P_n^m(\cos\theta_1) + \sum_{n=m+1}^\infty \Lambda_2(a,n,m,\omega)\kappa(n,m)\csc\theta_1 P_{n-1}^m(\cos\theta_1) + \sum_{n=m}^\infty \Lambda_2(a,n,m,\omega)\gamma(n,m)\csc\theta_1 P_{n+1}^m(\cos\theta_1) = 0.$$
$$\tag{C2}$$

Changing the order of summation, and renaming some indices, Eq. (C2) can be rewritten as

$$\sum_{n=m}^{\infty} \{ i\, m\Lambda_1(a,n,m,\omega) + \Lambda_2(a,n+1,m,\omega)\kappa(n+1,m)$$
$$+ \Lambda_2(a,n-1,m,\omega)\gamma(n-1,m)(1-\delta_{nm})\} \csc\theta_1 P_n^m(\cos\theta_1) = 0.$$

Lastly, the classical orthogonality property of the associated Legendre functions (see Eq. 12.104 in Ref. [48]) can readily be implemented to obtain

$$i\, m\Lambda_1(a,n,m,\omega) + \Lambda_2(a,n+1,m,\omega)\kappa(n+1,m) + \Lambda_2(a,n-1,m,\omega)\gamma(n-1,m)(1-\delta_{nm}) = 0,$$

which is the same as Eq. (12b). Similarly, following the above procedure, satisfaction of the boundary condition $\sigma_{r\phi}(r_1=a,\theta_1,\phi,\omega)=0$ yields

$$i\, m\Lambda_2(a,n,m,\omega) - \Lambda_1(a,n+1,m,\omega)\kappa(n+1,m) - \Lambda_1(a,n-1,m,\omega)\gamma(n-1,m)(1-\delta_{nm}) = 0,$$

which is the same as Eq. (12c).

Appendix D

$$Z_{m\nu}^{mn}(e,\omega) = \sum_{\sigma=|n-\nu|}^{\nu+n,2} (-i)^{\sigma}(2\nu+1)\bar{a}(m,n,-m,\nu,\sigma)j_{\sigma}(\alpha e),$$

$$Q_{m\nu}^{mn}(e,\omega) = \sum_{\sigma=|n-\nu|}^{\nu+n,2} (-1)^{m}i^{\nu+\sigma-n}a(n,\nu,\sigma)\bar{a}(m,n,-m,\nu,\sigma)j_{\sigma}(\beta e),$$

$$R_{m\nu}^{mn}(e,\omega) = \sum_{\sigma=|n-\nu|}^{\nu+n,2} (-1)^{m+1}i^{\nu+\sigma-n}b(n,\nu,\sigma)\tilde{a}(m,n,-m,\nu,\sigma-1)j_{\sigma}(\beta e),$$

where

$$a(n,\nu,\sigma) = [2\nu(\nu+1)(2\nu+1)+(\nu+1)(\nu+n-\sigma)(n+\sigma-\nu+1)-n(n+\nu+\sigma+2)]/[2\nu(\nu+1)]$$
$$b(n,\nu,\sigma) = [(\nu+n+\sigma+1)(\sigma+\nu-n)(n+\sigma-\nu)(n+\nu-\sigma+1)]^{1/2}(2\nu+1)/[2\nu(\nu+1)]$$

$$\bar{a}(m,n,-\mu,\nu,\sigma) = (-1)^{m}\sqrt{(2\sigma+1)(2\nu+1)(2n+1)/(4\pi)} \begin{pmatrix} n & \nu & \sigma \\ 0 & 0 & 0 \end{pmatrix} \begin{pmatrix} n & \nu & \sigma \\ -m & \mu & m-\mu \end{pmatrix},$$

$$\tilde{a}(m,n,-\mu,\nu,\sigma,\sigma-1) = (-1)^{m}\sqrt{(2\sigma+1)(2\nu+1)(2n+1)/(4\pi)} \begin{pmatrix} n & \nu & \sigma \\ 0 & 0 & 0 \end{pmatrix} \begin{pmatrix} n & \nu & \sigma-1 \\ -m & \mu & m-\mu \end{pmatrix}.$$

where

$$\begin{pmatrix} n & \nu & p \\ m & \mu & q \end{pmatrix}$$

is the Winger 3j symbol [12].

Appendix E

$$A_{nm}(e,\omega) = \sum_{\nu=m}^{\infty} a_{\nu m} Z_{mn}^{m\nu}(e,\omega),$$

$$B_{nm}(e,\omega) = \sum_{\nu=m}^{\infty} b_{\nu m} Z_{mn}^{m\nu}(e,\omega),$$

$$C_{nm}(e,\omega) = \sum_{\nu=m}^{\infty} c_{\nu m} Q_{mn}^{m\nu}(e,\omega) + e_{\nu m} R_{mn}^{m\nu}(e,\omega),$$

$$D_{nm}(e,\omega) = \sum_{\nu=m}^{\infty} d_{\nu m} Q_{mn}^{m\nu}(e,\omega) + f_{\nu m} R_{mn}^{m\nu}(e,\omega),$$

$$E_{nm}(e,\omega) = \sum_{\nu=m}^{\infty} c_{\nu m} R_{mn}^{m\nu}(e,\omega) + e_{\nu m} Q_{mn}^{m\nu}(e,\omega),$$

$$F_{nm}(e,\omega) = \sum_{\nu=m}^{\infty} d_{\nu m} Q_{mn}^{m\nu}(e,\omega) + f_{\nu m} R_{mn}^{m\nu}(e,\omega). \tag{E1}$$

References

[1] M.S. Qatu, Recent research advances in the dynamic behavior of shells: 1989-2000, Part 1: Laminated composite shells, *Applied Mechanics Reviews* (55) (2002) 325–351.

[2] M.S. Qatu, Recent research advances in the dynamic behavior of shells: 1989–2000, Part 2: Homogeneous shells, *Applied Mechanics Reviews* (55) (2002) 415–435.

[3] A.W. Leissa, *Vibration of Shells (NASA SP-288)*, US Government Printing Office, 1973.

[4] A.E.H. Love, *A Treatise on the Mathematical Theory of Elasticity*, Dover, New York, 1944.

[5] H. Lamb, On the vibrations of an elastic sphere, *Proceedings London Mathematical Society* 13 (1882) 189–212.

[6] C. Chree, The equations of an isotropic elastic solid in polar and cylindrical coordinates, their solutions and applications, *Transactions of the Cambridge Philosophical Society* 14 (1889) 250–309.

[7] Y. Sato, T. Usami, Basic study on the oscillation of a homogeneous elastic sphere; part I, frequency of the free oscillations, *Geophysics Magazine* 31 (1962) 15–24.

[8] Y. Sato, T. Usami, Basic study on the oscillation of a homogeneous elastic sphere; part II, distribution of displacement, *Geophysics Magazine* 31 (1962) 25–47.

[9] A.H. Shah, C.V. Ramakrishnan, S.K. Datta, Three dimensional and shell theory analysis of elastic waves in a hollow sphere, Part I. Analytical foundation, *Journal of Applied Mechanics* 36 (1969) 431–439.

[10] E.R. Lapwood, T. Usami, *Free Oscillations of the Earth*, Cambridge University Press, 1981.

[11] S. Hosseini-Hashemi, J.S. Anderson, Orthogonality and normalization of torsional modes of vibration of solid elastic spheres, *Journal of Sound and Vibration* 121 (1988) 511–524.

[12] P.R. Heyliger, A. Jilani, The free vibrations of inhomogeneous elastic cylinders and spheres, *International Journal of Solids and Structures* 29 (1992) 2689–2708.

[13] N. Kumbasar, Free vibration of thick spherical shells, *Bulletin of the Technical University of Istanbul* 41 (1988) 273–283.

[14] Y.C. Chang, L Demkowicz, Vibrations of a spherical shell comparison of 3-D elasticity and Kirchhoff shell theory results, *Texas Institute for Computational and Applied Mathematics* 2 (1995) 187–206.

[15] O.G. McGee, S.C. Spry, A three-dimensional analysis of the spheroidal and torsional elastic vibrations of thick-walled spherical bodies of revolution, *International Journal for Numerical Methods in Engineering* 40 (1997) 1359–1382.

[16] K.T. Chau, Toroidal vibrations of anisotropic spheres with spherical isotropy, *Journal of Applied Mechanics* 65 (1998) 59–65.

[17] G. Buchanan, B. Rich, Effect of boundary conditions on free vibration of thick isotropic spherical shells, *Journal of Vibration and Control* 8 (2002) 389–403.

[18] L. Saviot, D.B. Murray, Longitudinal versus transverse spheroidal vibrational modes of an elastic sphere, *Physical Review B* 72 (2005) 205433–205439.

[19] T.A. Duffey, J.E. Pepin, A.N. Robertson, M.L. Steinzig, K. Coleman, Vibrations of complete spherical shells with imperfections, *Journal of Vibration and Acoustics* 129 (2007) 363–370.

[20] B. Friedman, J. Russek, Addition theorems for spherical waves, *Quarterly of Applied Mathematics* 12 (1954) 13–23.

[21] S. Stein, Additions theorems for spherical wavefunctions, *Quarterly of Applied Mathematics* 19 (1961) 15–24.

[22] O.R. Cruzan, Translational addition theorems for spherical vector wave functions, *Quarterly of Applied Mathematics* 20 (1962) 33–40.

[23] V.T. Golovchan, Oscillation of a spherical of variable thickness shell, *Translated from Prikladnaya Mekhanika* 10 (1974) 9–13.

[24] J.D. Kanellopoulos, J.G. Fikioris, Acoustic resonant frequencies in an eccentric spherical cavity, *The Journal of the Acoustical Society of America* 64 (1978) 286–297.

[25] J.A. Roumeliotis, J.D. Kanellopoulos, J.G. Fikioris, Acoustic resonance frequency shifts in a spherical cavity with an eccentric inner small sphere, *Journal of the Acoustical Society of America* 90 (1991) 1144–1148.

[26] J.A. Roumeliotis, J.D. Kanellopoulos, Acoustic eigenfrequencies and modes in a soft-walled spherical cavity with an eccentric inner small sphere, *Journal of Franklin Institute* 329 (1992) 727–735.

[27] J.A. Rourneliotis, J.D. Kanellopoulos, John G. Fikioris, Resonant frequencies in an electromagnetic spherical cavity with an eccentric inner eccentrically small sphere, *Electromagnetics* 12 (1992) 155–170.

[28] J.A. Roumeliotis, N.B. Kakogiannos, J.D. Kanellopoulos, Scattering from a sphere of small radius embedded into a dielectric one, *IEEE Transactions on Microwave Theory and Techniques* 43 (1995) 155–168.

[29] P.G. Cottis, M.A Moyssidis, Complex resonances of a conducting sphere eccentrically coated by a dielectric one, *Journal of Electromagnetic Waves and Applications* 11 (1997) 3–20.

[30] A. Charalambopoulos, D.I. Fotiadis, C.V. Massalas, Frequency spectrum of the bispherical hollow system: the case of the nonuniform thickness human skull, *Acta Mechanica* 130 (1998) 249–278.

[31] M.P. Ioannidou, D.P. Chrissoulidis, Electromagnetic-wave scattering by a sphere with multiple spherical inclusions, *Journal of the Optical Society of America A: Optics and Image Science, and Vision* 19 (2002) 505–512.

[32] G. Videen, Seismic scattering from a spherical inclusion eccentrically located within a homogeneous, spherical host: theoretical derivation, *Waves Random Media* 13 (2003) 177–190.

[33] S.M. Hasheminejad, M. Azarpeyvand, Energy distribution and radiation loading of a cylindrical source suspended within a nonconcentric fluid cylinder, *Acta Mechanica* 164 (2003) 15–30.

[34] A.P. Moneda, D.P. Chrissoulidis, Dyadic Green's function of a sphere with an eccentric spherical inclusion, *Journal of the Optical Society of America A* 24 (2007) 1695–1703.

[35] G. Han, Y. Han, J. Liu, Y. Zhang, Scattering of an eccentric sphere arbitrarily located in a shaped beam, *Journal of the Optical Society of America B: Optical Physics* 25 (2008) 2064–2072.

[36] B. Yan, X. Han, K. Fang Ren, Scattering of a shaped beam by a spherical particle with an eccentric spherical Inclusion, *Journal of Optics A: Pure and Applied Optics* 11 (2009) art. no. 015705.

[37] T. Hirai, Analysis of natural vibrations of a spherical shell with variable thickness, *The Journal of the Acoustical Society of America* 86 (1989) 1864–1875.

[38] P.G. Young, S.M. Dickinson, Free vibration of a class of solids with cavities, *International Journal of Mechanical Sciences* 36 (1994) 1099–1107.

[39] Z. Martinec, Semi-analytical solution for viscoelastic relaxation in eccentrically nested spheres induced by surface toroidal traction, *Pure and Applied Geophysics* 166 (2009) 1167–1197.

[40] J. Jellison, H.R. Kess, D.E. Adams, D.C. Nelson, Vibration-based NDE technique for identifying non-uniformities in manufacture parts with degeneracies, *Proceedings of IMECE*, New Orleans, LA, 2002, pp. 621–628.

[41] M. de Billy, A.C. Hladky-Hennion, On the splitting of aspherical structure submitted to an acoustic polarized excitation, *Ultrasonics* 43 (2004) 27–34.

[42] J.G. Minonzio, F.D. Philippe, C. Prada, M. Fink, Characterization of an elastic cylinder and an elastic sphere with the time-reversal operator: application to the sub-resolution limit, *Inverse Problems* 24 (2008) 24pp art. no. 025014.

[43] J.H. Kang, A.W. Leissa, Three-dimensional vibrations of thick spherical shell segments with variable thickness, *International Journal of Solids and Structures* 37 (2000) 4811–4823.

[44] A.G. Gorshkov, D.V. Tarlakovskii, A.M. Shukurov, Unsteady vibrations of an elastic medium bounded by two eccentric spherical surface, *Journal of Applied Mathematics and Mechanics* 58 (1994) 275–282.

[45] Y.H. Pao, C.C. Mow, *Diffraction of Elastic Waves and Dynamics Stress concentration*, Crane Russak, New York, 1973.
[46] N.G. Einspruch, E.J. Witterholt, R. Truell, Scattering of a plane transverse wave by a spherical obstacle in an elastic medium, *Journal of Applied Physics* 5 (1960) 806–818.
[47] M. Abramowitz, I.A. Stegun, *Handbook of Mathematical Functions*, Dover Publications, 1965.
[48] G.B. Arfken, J.W. Hans, F. Harris, *Mathematical Methods for Physicists*, Harcourt Academic, San Diego, CA, 2001.
[49] H. Sato, Y. Shindo, Multiple scattering of plane elastic waves in a particle-reinforced-composite medium with graded interfacial layers, *Mechanics of Materials* 35 (2003) 83–106.
[50] S. Wolfram, *Mathematica: a System for Doing Mathematics by Computer*, second ed, Addison Wesley Publishing Company, Reading, MA, 1991.
[51] ABAQUS, Analysis User's Manual Version 6.6 On-line Documentation.